

THESIS FOR THE DEGREE OF LICENTIATE OF PHILOSOPHY

Raster Image Analysis of Diffusion via Single Particle Methods

MARCO LONGFILS

CHALMERS |  **GÖTEBORGS UNIVERSITET**

*Division of Applied Mathematics and Statistics
Department of Mathematical Sciences*

CHALMERS UNIVERSITY OF TECHNOLOGY AND UNIVERSITY OF
GOTHENBURG
Göteborg, Sweden 2017

Raster Image Analysis of Diffusion via Single Particle Methods
Marco Longfils

© Marco Longfils, 2017.

Department of Mathematical Sciences
Chalmers University of Technology and University of Gothenburg
SE-412 96 GÖTEBORG, Sweden
Phone: +46 (0)31 772 3574

Author e-mail: `longfils@chalmers.se`

Typeset with \LaTeX .
Department of Mathematical Sciences
Printed in Göteborg, Sweden 2017

Raster Image Analysis of Diffusion via Single Particle Methods

Marco Longfils

*Department of Mathematical Sciences
Chalmers University of Technology and University of Gothenburg*

Abstract

Soft biomaterials are widely used in many application areas, spanning from packaging materials to pharmaceuticals. To enhance their functionalities, understanding the interplay between microstructure and mass transport properties in these materials is fundamental. Consequently, there is a growing need to introduce new and improve existing methods for estimating mass transport heterogeneity in materials with high spatial resolution. In this work, statistical methods are developed for mapping mass transport locally based on raster images collected using a confocal laser scanning microscope. The methods introduced resemble single particle tracking methods, where molecules are identified using image analysis techniques and followed in successive frames of a video to measure their diffusive mobility. Both a maximum likelihood and a centroid-based method have been applied to locate particles and hence to estimate the diffusion coefficient. The method has been generalized to analyse mixtures of particles having different diffusion coefficients. The single particle approach allows to reveal and study the entire distribution of diffusion coefficients, enabling to examine heterogeneous systems. Further, for the case of particle mixtures, a simple criterion for model selection, i.e. the number of components, is proposed.

Keywords: confocal laser scanning microscopy, diffusion, image correlation spectroscopy, raster scan, single particle tracking.

List of appended papers

The following papers are included in this thesis:

Paper I. **Longfils, M.**, Schuster, E., Lorén, N., Särkkä, A., and Rudemo, M.
Single particle raster image analysis of diffusion. *Journal of Microscopy*,
doi:10.1111/jmi.12511.

Paper II. **Longfils, M.**, Röding, M., Altskär A.; Schuster, E., Lorén, N.,
Särkkä, A., and Rudemo, M. Raster image analysis of diffusion for par-
ticle mixtures. *Manuscript*.

My contribution to the appended papers:

Paper I: I co-developed and implemented the single particle raster image anal-
ysis. Moreover, I carried out the simulation study as well as the analysis
of the experimental data. I also participated in the data collection and
did most of the writing for the publication.

Paper II: I implemented both single particle raster image analysis and raster
image correlation spectroscopy in the case of mixtures of particles. More-
over, I carried out the simulation study as well as the analysis of the
experimental data. I also did most of the writing for the publication.

Acknowledgements

First and foremost, I would like to thank my supervisor Aila Särkka for her continuous support in every aspect of my studies. I dropped by your office far too many times and you always had time for me. I would also like to thank Mats Rudemo, for the very interesting discussion we had about my project. Furthermore, I thank Sergei Zuyev, for teaching me most of what I know about probability and the exciting discussion we had. I would also like to thank Magnus Röding, who just recently joined the team of my supervisors and had already contributed considerably to my growth as a researcher.

A big thanks goes to Niklas Lorén, Erich Schuster, and Annika Altskär from RISE for creating a fascinating and challenging interdisciplinary research environment, and for providing interesting microscopy data without which my work would not be possible. I am also grateful to my colleagues for making the department an enjoyable workplace.

Last, but not least, I am grateful to my parents and my brother for their love and constant support. Everything I have reached so far I owe to you.

Financial support from the Swedish Foundation for Strategic Research, SSF, is highly appreciated.

Contents

1	Introduction	1
2	Diffusion	2
2.1	Microscopy data	4
3	Methods to estimate diffusion	6
3.1	Image Correlation Spectroscopy	6
3.1.1	Raster Image Correlation Spectroscopy	8
3.2	Single Particle Tracking	11
3.2.1	Single Particle Raster Image Analysis	13
4	Summary of papers	15
4.1	Paper I: Single particle raster image analysis of diffusion	15
4.2	Paper II: Raster image analysis of diffusion for particle mixtures	17
5	Future work	18
A	Derivation of RICS correlation function for pure diffusion	20
	References	28

1 Introduction

For many applications, ranging from packaging materials to pharmaceuticals, creating biomaterials with tuned mass transport functionalities is a critical effort. Therefore, understanding the microstructure - mass transport relationship is highly important. In order to successfully create such materials, measurement methods need to resolve the mass transport (diffusion in our settings) properties at the length scale of the material structures. This requires performing measurements with (sub-)micrometer spatial resolution. The aim of this work is to develop a new, high accuracy statistical method to map mass transport heterogeneity at a (sub-)micrometer scale and further promote existing microscopy methods to determine mass transport.

In this work, we concentrate on pure diffusion and how to estimate diffusion coefficients, both when there is only one (monodisperse) and when there are several (polydisperse) diffusing coefficients. The organization of this thesis is as follows: In Section 2, I give an introduction to molecular diffusion, which is the main interest of the two appended papers. Since all the experimental data analyzed in this study were collected with a confocal laser scanning microscope, I briefly introduce the principles of confocal microscopy in Section 3. Then, in Section 4, I give an overview of two large families of available methodologies employed to study diffusion, Image Correlation Spectroscopy and Single Particle Tracking. In particular, as the method we introduced called Single Particle Raster Image Analysis is the main focus of the two appended papers, only a brief description of this method will be given in the introduction of this thesis. Additionally, more details are provided for the Raster Image Correlation Spectroscopy technique with exhaustive computation of the correlation function presented in the Appendix A. In Section 4, the appended papers are summarised and in section 5 possible topics of study in future work are presented.

2 Diffusion

Diffusion is the migration or movement of particles due to random motion driven by thermal energy. There are three main perspectives on how we can look at diffusion: Fick's law, the Einstein-Smoluchowski relation, and the Wiener process. To describe the three points of view, we start by considering pure diffusion of particles with a single diffusion coefficient in a homogeneous medium. In this case, the diffusion coefficient of all the particles will be the same, as the system is monodisperse, and constant over space, as the medium in which diffusion takes place is homogeneous. Let $C(r, t)$ and $\delta C(r, t)$, respectively, be the concentration of particles and the deviation from the average concentration at the position $r \in \mathbb{R}^3$ and time $t \in [0, \infty)$. The temporal evolution of such a system is described by Fick's (second) law of diffusion,

$$\frac{\partial u(r, t)}{\partial t} = D\nabla^2 u(r, t), \quad (2.1)$$

where $D > 0$ is the diffusion coefficient and ∇^2 is the Laplacian operator. Fick's law is satisfied by both the concentration $C(r, t)$ and the deviation from the average concentration $\delta C(r, t)$, and predicts how these quantities change with time. The physical properties of diffusion are characterised by a density function $P(r, t)$, called the propagator. The propagator specifies the probability density of finding a particle located at r at time t when the particle was at the origin at time zero. The propagator is given by

$$P(r, t) = \frac{1}{(4\pi Dt)^{\frac{3}{2}}} e^{-\frac{\|r\|^2}{4Dt}}. \quad (2.2)$$

The propagator fully describes the type of movement exhibited by the particles and is directly involved in the correlation function used by Raster Image Correlation Spectroscopy, see the derivation of Equation (A.7) in Appendix A. For flow with a velocity vector $V = (V_x, V_y, V_z)$, the propagator takes the form

$$P(r, t) = \delta(r_x - V_x t)\delta(r_y - V_y t)\delta(r_z - V_z t), \quad (2.3)$$

where $\delta(x - y)$ equals one if $x = y$ and zero otherwise. There are more propagators which have been used for different modes of motion, e.g. for directed diffusion and anomalous diffusion. The former is the superposition of flow and pure diffusion, while the latter defines generally a deviation from pure diffusion. Anomalous diffusion is characterised by the displacement having a second

moment which follows a power law $\sim t^\alpha$ as a function of time, and usually is classified as subdiffusion for $\alpha < 1$ or superdiffusion $\alpha > 1$. This type of motion has been observed in cell membranes as a result of both obstacles and binding kinetics. As described in Bouchard & Georges (1990), one way to model anomalous diffusion is to consider particles performing a random walk where the jumps are drawn from a broad distribution or show long range correlation. Thus, the usual central limit theorem does not hold anymore and the law of Brownian motion, corresponding to pure diffusion, is not valid. Fick's law describes the macroscopic properties of diffusion, as it defines how the concentration of particles changes in time. On the other hand, the following interpretation of diffusion in terms of the Wiener process provides a microscopic view of the process, as it gives a description of diffusion in terms of the motion of the single particles. Molecules undergoing diffusion are mathematically modelled as particles moving according to a Brownian motion, compare Equation (2.2), where the variance of the Gaussian increments is proportional to the interval of time considered and the constant of proportionality is the diffusion coefficient (up to a dimensionality constant). Formally, consider n diffusing particles and let $X_i(t) = (X_i^1(t), \dots, X_i^d(t))$, $i = 1, \dots, n$, denote the vector of the position in \mathbb{R}^d of the i -th particle at time t . Then, X_i^1, \dots, X_i^d are independent translated copies of Wiener processes W defined by:

1. $W_i(0) = 0$;
2. $W_i(t) - W_i(s) \sim N(0, 2D_i(t - s)) \forall t > s \geq 0$, where D_i is the diffusion coefficient of the i -th particle;
3. Increments of W_i for nonoverlapping time intervals are independent.

The last perspective on diffusion is given by the Einstein-Smoluchowski relation. The Einstein-Smoluchowski relation was firstly derived by Einstein (1905) and a year later independently by Smoluchowski (1906), and it links the macroscopic diffusion coefficient D to the microscopic information about the mean square displacement

$$\mathbb{E}[(X(t + \delta t) - X(t))^2] = 2dD\delta t. \quad (2.4)$$

The above representations of diffusion are exploited by image correlation techniques and single particle methods. In the first family, as particles appear as bright spots in the image due to the fluorescent labelling, the correlation between and/or within images is coupled to the probability of finding the same particle again at some spatiotemporal lag, which in turn is related to the propagator. In single particle methods, the displacements $X_i(t + \delta t) - X_i(t)$ are directly estimated for some fixed temporal lag δt , for example the time between

consecutive images. Then, the diffusion coefficient can be estimated from the moments of the displacements.

In a more general case, particles can interact chemically with each other or spatially with particular structures like binding sites. We consider here a solution of particles having m distinct diffusion coefficients and denote by $C_j(r, t)$ and $\delta C_j(r, t)$ respectively the concentration of the j -th component and the deviation from the average concentration, for components $j = 1, \dots, m$. Moreover, denote by D_j , $j = 1, \dots, m$, the diffusion coefficient of the j -th component. Near equilibrium, the system evolves according to the so called reaction-diffusion equation

$$\frac{\partial \delta C_j(r, t)}{\partial t} = D_j \nabla^2 \delta C_j(r, t) + \sum_{k=1}^m K_{jk} \delta C_k(r, t), \quad (2.5)$$

where the first term on the right hand side accounts for diffusion and the second describes changes due to interaction. In this work, we will restrict ourself to diffusion, leaving interaction to be a possible subject of future studies.

2.1 Microscopy data

All data considered here were collected with a confocal laser scanning microscope (CLSM), see Pawley (2006) for a comprehensive introduction to the subject. The CLSM works by passing a laser beam through an illumination aperture which is then focused by an objective lens into a small area of the sample, see Figure 2.1. If fluorophores are present there and are illuminated with the proper wavelength, they emit light. This light then passes through a semi-transparent mirror, the dichroic mirror, which reflects it towards the detection system. At this point, light passes through the emission filter, which separates the fluorescent light from the laser light reflected by the sample. For every pixel in the region of interest, the number of photons emitted from the fluorophores in the sample or an intensity value is recorded by a photon counter or a photo multiplier tube. A pinhole aperture in front of the detector is used to exclude fluorescence from the out-of-focus planes. In Figure 2.1 the light beams from the sample that come from out-of-focus planes, represented as dashed and dotted lines, are stopped by the pinhole and not collected by the detector. Hence, confocal microscopy provides a "well-isolated" plane. Confocal microscopes allow detection of fluorescent molecules with a good spatial resolution.

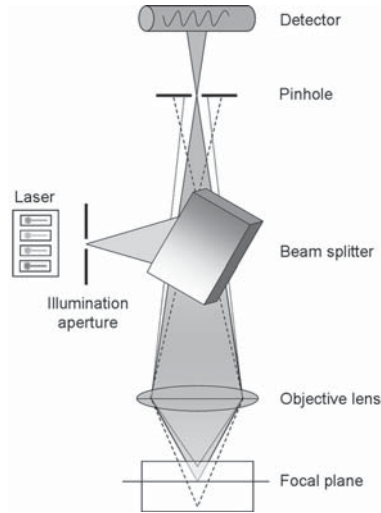


Figure 2.1: Schematic illustration of confocal laser scanning microscopy.

In the experiments, fluorescent microspheres have been used as probes to study diffusion. We considered four different diameters for the microspheres (100, 175, 500, 1000 nm) where the smallest size covers the subresolution domain, while the largest size is nearly the size of a living cell. Within each size considered, the standard deviation of the diameter, typically around 2-3% of the size, is remarkably small, which allows us to ideally consider the particles as uniform in terms of size and shape. The homogeneity of the microspheres is fundamental in ensuring that any variation in their motion is due to the surrounding structure. Moreover, the beads have been stained with four different fluorescent dyes. Thus they will be visible only if excited with one of the corresponding four well-separated wavelengths. In applications, we can use different colors to label the structure or important immobile features in the sample and the particles. By observing their motion using different detectors, we can easily separate the background from the diffusing microspheres. The fluorescent dye is used to stain the particles in such a way that the fluorophore distribution is uniform over the volume of each microsphere. In a confocal image an immobilized fluorescent microsphere appears as a bright round object, the radius of which depends on the distance of the particle to the focal plane and the size of the particle. The closer the particle is to the focal plane, the larger the radius will be, see for example the top left plot in Figure 3.3.

3 Methods to estimate diffusion

In this work, we focus on two major methodologies to study diffusion, the Image Correlation Spectroscopy (ICS) and Single Particle Tracking (SPT) techniques. As there exist many other noteworthy methods, we will briefly describe some of them here. Fluorescence Recovery After Photobleaching (FRAP) was first used to analyze the mobility of individual molecules within a cell membrane. In FRAP Lorén *et al.* (2015), a fluorescent probe is introduced in the sample, a cell or a soft biomaterial. Then, a high intensity laser bleaches for a short time the fluorescence in the region of interest and a sequence of images is collected to follow the recovery rate of the fluorescence. Over time, non-bleached probes will diffuse into the region of interest, while the bleached ones will diffuse out of it. Thus, from the recovery of the fluorescence information about diffusion can be retrieved.

As ICS methods have been a part of this study, it is worth to spend some time describing its precursor, namely Fluorescence Correlation Spectroscopy (FCS). In an FCS experiment, a small volume of the sample is illuminated by a stationary light source and the fluorescence from particles is recorded. Since particles are allowed to diffuse in and out of the observed volume and may undergo chemical and physical processes, fluctuations in the signal will arise. By recording the fluorescence intensity over a time period, a time series will be generated. The temporal autocorrelation function of this time series will be distinct for different types of motion of the particles and interactions like binding. Thus, by analyzing the shape of the autocorrelation function, we can determine the behaviour of the particles in the sample and extract parameters of interest like the diffusion coefficient or the average binding time.

3.1 Image Correlation Spectroscopy

We present here a brief overview of Image Correlation Spectroscopy (ICS) and introduce Raster Image Correlation Spectroscopy (RICS) in more detail. Image Correlation Spectroscopy is a unifying term for a group of fluorescence fluctuation spectroscopy techniques based on analysis of fluorescence microscopy image data. ICS methods are subdivided according to whether fluorescence fluctuation information in space and/or time is analysed within the image se-

ries. Temporal ICS (TICS) Kulkarni *et al.* (2005) analyses fluorescence fluctuations in time recorded in the pixels of an image time series. Spatiotemporal ICS (STICS) Hebert *et al.* (2005) considers information in both space and time. An innovative method is Raster scan ICS (RICS) Digman *et al.* (2005); Brown *et al.* (2008); Gielen *et al.* (2009), which like STICS considers spatiotemporal correlations, but gains access to a faster timescale by exploiting the rapid pixel-to-pixel sampling in a laser scanning microscope. We should point out that many other methods fall under the ICS family, as kICS (k-reciprocal Image Correlation Spectroscopy) Kolin *et al.* (2006), ICCS (Image Cross-Correlation Spectroscopy) Comeau *et al.* (2006) and variants of them. All varieties of ICS are based on an image or image time series recorded using fluorescence microscopy, such as confocal laser scanning microscopy (CLSM) or Total Internal Reflection Microscopy (TIRF). In all pixels of an image the output of the photomultiplier tube or bin counts from a CCD camera are registered. For example, in the case of a photon counting detector, the pixel intensity represents an actual count of detected photons. The key feature that ICS methods take advantage of is that the intensity of a point fluorescent source will be spread out upon detection due to the diffraction of light. The diffraction pattern is described by the point spread function (PSF). The PSF is assumed to be a three-dimensional Gaussian function for a confocal microscope with different axial (z -direction) and lateral (xy -plane) standard deviations. Thus, if the pixel size is smaller than the diameter of the PSF, spatial correlation will be introduced between adjacent pixels of the image. The effect of the PSF is shown in Figure 3.1.

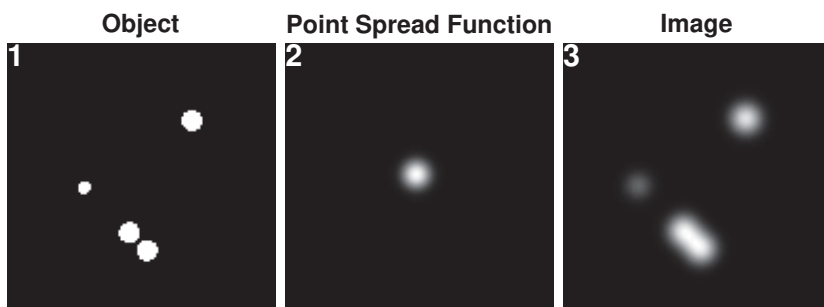


Figure 3.1: Image describing the effect of the point spread function. 1: the object of interest is depicted; 2: the point spread function is plotted. 3: the image as recorded by the microscope is shown, where the image is the result of the convolution of the other two images.

3.1.1 Raster Image Correlation Spectroscopy

In this section we describe RICS in more detail, and in particular we focus on the case of line scanning, while many considerations apply also in the case of circular scanning. In RICS, each image is scanned pixel-by-pixel and line-by-line through the movement of the focal observation volume according to a raster pattern. This particular sampling pattern introduces time information within the image. The scanning of the sample is executed as shown in Figure 3.2. The observation volume is placed on the first (from left to right) pixel of the image which is scanned. Then, after the pixel dwell time τ_p , the second pixel in the first line is scanned. Scanning pixel-by-pixel, the first line of the image will be collected. In the next step, after the line time τ_l , the observation volume is retraced to the beginning of the second line of pixels. At this point, the second line is recorded, and by iterating this process the whole image will be sampled. Typically in a RICS measurement, adjacent pixels in the x -direction are scanned within a microsecond, and adjacent pixels in the y -direction are scanned within a millisecond.

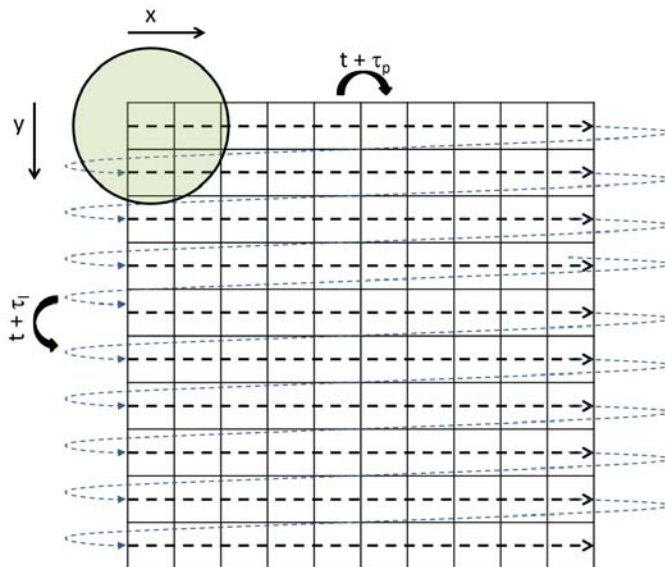


Figure 3.2: Movement of the scanning beam according to the raster scan pattern used in RICS. The scanning time between adjacent pixels in the x - and y -directions are τ_p and τ_l , and $\tau_p \ll \tau_l$.

In all correlation spectroscopy techniques, the signal fluctuations with respect to the average is calculated as:

$$\delta F(r, t) = F(r, t) - \langle F(r, t) \rangle$$

where $F(r, t)$ is the signal in r at time t , $\delta F(r, t)$ is the fluctuation of the signal and $\langle \cdot \rangle$ denotes averaging. The normalised correlation of the fluctuations, $G(\rho, \tau)$, is given by:

$$G(\rho, \tau) = \frac{\langle \delta F(r, t) \delta F(r + \rho, t + \tau) \rangle}{\langle F(r, t) \rangle^2} = \frac{\langle F(r, t) F(r + \rho, t + \tau) \rangle}{\langle F(r, t) \rangle^2} - 1$$

where $\rho = (\rho_x, \rho_y)$ and τ are the spatial and temporal shifts. It should be noted that $G(\rho, \tau)$ is not exactly a correlation function, but a normalized covariance function where the maximum of $G(\rho, \tau)$ scales as the inverse of the average number of particles in the observation volume $\langle N \rangle$. However, in the literature it is referred to as the correlation function, so we will use this name. The correlation function for RICS in the case of pure diffusion, where the lags are $\tau = \tau_p |\xi| + \tau_l |\psi|$ and $\rho_x = S\xi$, $\rho_y = S\psi$, where S is the pixel size and ξ and ψ are the x - and y -axis spatial increments in the number of pixels, is given by:

$$G(\xi, \psi) = \frac{1}{\langle N \rangle} e^{\left[-\frac{(S\xi)^2 + (S\psi)^2}{w_0^2 + 4D(\tau_p |\xi| + \tau_l |\psi|)} \right]} \left(1 + \frac{4D(\tau_p |\xi| + \tau_l |\psi|)}{w_0^2} \right)^{-1} \times \left(1 + \frac{4D(\tau_p |\xi| + \tau_l |\psi|)}{w_z^2} \right)^{-\frac{1}{2}}. \quad (3.1)$$

Some examples are plotted in Figure 3.3 and more details are provided in the Appendix.

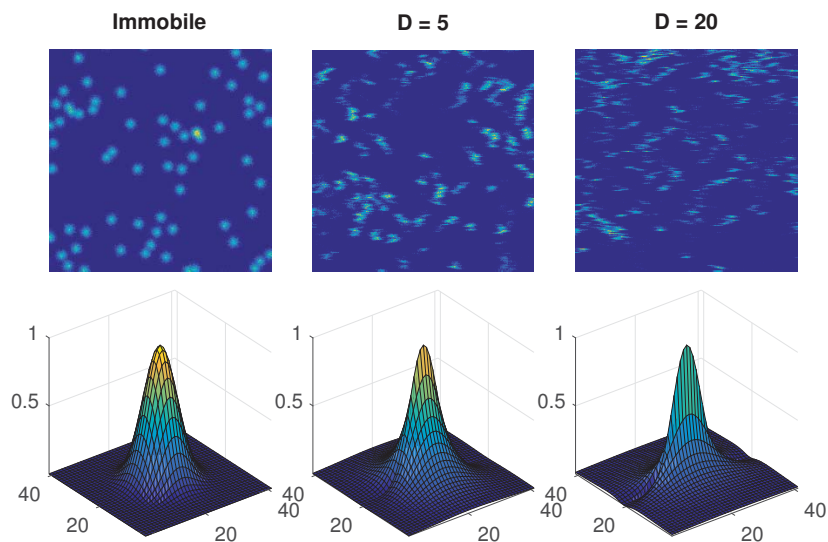


Figure 3.3: Top: Examples of a typical RICS image for immobile particles (left), diffusing particles with $D = 5 \mu\text{m}^2 \text{s}^{-1}$ (middle), and diffusing particles with $D = 20 \mu\text{m}^2 \text{s}^{-1}$ (right). Bottom: theoretical autocorrelation functions for the different cases.

Assume we have n images with resolution $K \times K$ from which we want to estimate diffusion. Let $C(\xi, \psi, j)$ be the empirical correlation function relative to a shift of ξ pixels in the x -direction and ψ pixels in the y -direction, $1 \leq \xi, \psi \leq K$, of the j -th image, $1 \leq j \leq n$. In RICS, the estimation procedure obeys the following steps:

1. Compute $C(\cdot, \cdot, j)$ for all $1 \leq j \leq N$ via the Fast Fourier Transform algorithm;
2. To reduce the effect of noise, compute the average empirical correlation function of the stack of images

$$\hat{C}(\xi, \psi) = \frac{1}{n} \sum_{j=1}^n C(\xi, \psi, j)$$

3. Consider the following theoretical correlation function depending on the vector of parameters $\theta = (\langle N \rangle, D, O)$, respectively the average number of particles in the observation area, the diffusion coefficient and the offset of the correlation function:

$$G(\xi, \psi, \theta) = \frac{1}{\langle N \rangle} e^{\left[-\frac{(S\xi)^2 + (S\psi)^2}{w_0^2 + 4D(\tau_p|\xi| + \tau_l|\psi|)} \right]} \left(1 + \frac{4D(\tau_p|\xi| + \tau_l|\psi|)}{w_0^2} \right)^{-1} \times \quad (3.2)$$

$$\times \left(1 + \frac{4D(\tau_p|\xi| + \tau_l|\psi|)}{w_z^2} \right)^{-\frac{1}{2}} + O$$

where τ_p, τ_l, S are respectively the pixel dwell time, line time and pixel size.

4. Define the estimate $\hat{\theta}$ as the weighted least squares estimate of θ , i.e.

$$\hat{\theta} = \arg \min_{\theta} \sum_{\xi, \psi} w(\xi, \psi) \left[G(\xi, \psi, \theta) - \hat{C}(\xi, \psi) \right]^2,$$

where the weights $w(\xi, \psi) = \left(\sqrt{\text{Var}(\hat{C}(\xi, \psi))} \right)^{-1}$ are computed from the set of independent images.

3.2 Single Particle Tracking

Single Particle Tracking (SPT) was first introduced by Perrin (1909). Since then, many variants of this method have been introduced. However, they share the goal of investigating mass transport and the same measure of mass transport properties, even though the estimation techniques are different. One of the main advantages of SPT is that it gives access to the entire distribution of diffusion coefficients and subpopulations of particles, while other methodologies like FRAP or ICS average the behaviour of hundreds or thousands of diffusing particles. In SPT, a video or a sequence of frames is employed to track the motion of single particles. Here, a "particle" may be anything from a single molecule to a macromolecular complex or microsphere. Typical particles used as labels are fluorescent particles, such as latex beads or gold nanoparticles. The two main steps of the image analysis for SPT are: (i) particle detection, in which bright spots that stand out from the background are identified in some way and their positions estimated in every frame of the video, and (ii) particle linking, in which the detected spots are connected from one frame to the next to form tracks. Some examples of algorithms to localize particles are the centroid

algorithm, where the center of mass of the particle is used as a computationally simple and efficient estimate of its position, and the Gaussian fit algorithm, where a 2D or 3D Gaussian curve is fitted to the profile of the particle, and the mean provides a measure of the position. From the estimated trajectories one can extract the mean square displacement (MSD) which contains information about the type of motion. Let $x(t) \in \mathbb{R}^d$ be the position of the particle at time t . The MSD is defined as follows:

$$MSD(t) = \mathbb{E}[\|(x(s+t) - x(s))\|^2], \quad (3.3)$$

where $\|\cdot\|$ denotes the Euclidian norm in \mathbb{R}^d . By looking at the dependence of the MSD on time, one can distinguish different modes of motion and obtain estimates for the corresponding parameters. Some examples are:

$$\begin{aligned} MSD(t) &= 2dDt && \text{pure diffusion} \\ MSD(t) &= 2dDt^\alpha && \text{anomalous diffusion} \\ MSD(t) &= 2dDt + (\|V\|t)^2 && \text{directed diffusion} \end{aligned} \quad (3.4)$$

where D and V are, respectively, the diffusion coefficient and the velocity vector. The form of the MSD in Equation (3.4) for pure and directed diffusion is an immediate consequence of Equation (2.2) and Equation (2.3). In Figure 3.4, we plot the behaviour of the MSD for different modes of motion of the particles.

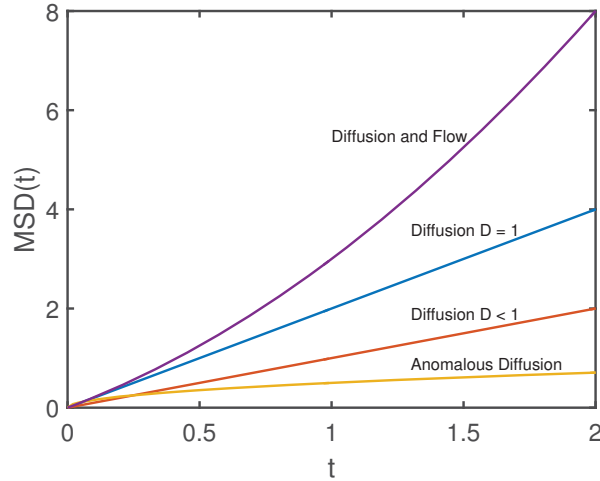


Figure 3.4: The mean square displacement as a function of time for simultaneous diffusion and flow, pure diffusion with $D = 1$ and $D < 1$, and anomalous diffusion.

3.2.1 Single Particle Raster Image Analysis

In typical SPT experiments, particles move negligibly within an image and appreciably between consecutive images. Thus, the motion is estimated from the position of a particle in consecutive images. In SPRIA, raster images are analysed where the scanning speed is such that the time between adjacent pixels in the x -direction is small (the pixel dwell time is in the order of a microsecond) while the time between adjacent pixels in the y -direction is large (the line dwell time is in the order of a millisecond). Hence, particles will move between consecutive lines in an image. More details are provided in the two appended papers, where the SPRIA method is introduced, discussed and validated on both simulated and experimental data. In this introduction we only recall briefly the main steps of SPRIA.

A particle is defined as an axis-parallel rectangle through a double threshold method. The first threshold is used to discriminate whether a local maximum of photon counts is an actual particle as opposed to noise, while the second threshold is adopted to delineate the boundary of the rectangle. In Figure 3.5 an identified particle is depicted, where pixels are colored based on their intensity in the image. Moreover, it can immediately be seen that two things in SPRIA are different from a typical SPT experiment: first, particles do not look round anymore as they are allowed to move while we are scanning them, producing a pattern of bright shifted lines; second, linking the successive positions of the particles to form tracks is more straightforward as the bright lines forming a particle, which corresponds to the different time points of the trajectory, tend to be connected, see Figure 3.5. Once a particle has been extracted as described above, its position in each line, i.e. in each time step of the trajectory, is estimated either by a maximum likelihood method based on the assumption of independently Poisson distributed photon counts in each pixel (Paper I) or by a centroid method (Paper II). In Figure 3.5, the trajectories estimated by both methods together with the true one are shown, indicating that SPRIA works well. Then, an estimate of the diffusion coefficient of the particle is obtained by using Equation (3.4) for pure diffusion when t is set to be the time τ_l between two consecutive lines. Finally, an overall estimate of one, or more in the case of particle mixtures, diffusion coefficient can be retrieved from the distribution of the diffusion coefficients of the single particles.

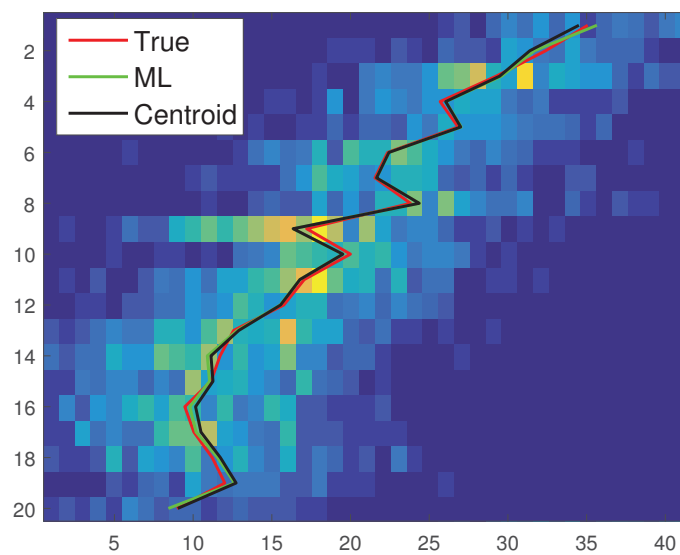


Figure 3.5: A simulated raster scan image of a 50nm particle showing the true trajectory (red), the corresponding estimated trajectory computed using the maximum likelihood method (green) introduced in Paper I, and the centroid based method (black) presented in Paper II.

4 Summary of papers

In this section, we introduce the methods used and summarise the results presented in the two appended papers. Regarding the simulated data analysed in this thesis, diffusion was reproduced by simulating discrete time Brownian motion of spheres in a box with periodic boundary conditions. Different settings of the scan rate, pixel size, pixel dwell time and line time were considered. In experimental data the motion of four (Paper I) and three (Paper II) different types of beads were recorded. A calibration step was performed on immobilized 175nm beads in a gelatin gel to obtain the lateral and axial waists of the point spread function for our experimental setup.

4.1 Paper I: Single particle raster image analysis of diffusion

The introduction of Raster Image Correlation Spectroscopy has led to a shift in the spatiotemporal analysis of dynamics in complex heterogeneous systems. By exploiting the time structure within single raster images, it is possible to increase the time resolution and resolve faster timescale dynamics by means of the quick pixel-to-pixel sampling. In this article we introduced Single Particle Raster Image Analysis (SPRIA), a single particle method to study raster images. The motivation of this study was to develop a method that could locally map mass transport properties. Previously, RICS has been applied to study heterogeneity Schuster *et al.* (2016), however as it gains strength from the averaging of many molecules, its spatial resolution is limited by the minimum size of the region of interest. Here, single particles are extracted using a double threshold method, where one thresholding is used to define which local maxima are particles and the second to separate the particles from the background. The maximum likelihood method is then employed to reconstruct the tracks of the molecules based on the assumption of pixelwise independent Poisson distributed photon counts. Two main problems were encountered when developing SPRIA: first, the symmetry of the likelihood with respect to the y and z coordinates made us restrict ourselves to estimate the diffusion coefficient only from the motion along the x -axis. Second, the raster scanning introduces a bias on the observed diffusion coefficient which is more significant the slower the scan rate is. This is due to the inherent preferential sampling of small compared to large

line-to-line displacements. We suggested a simulation based method to correct for this bias. Both on simulated and experimental data, SPRIA has shown to provide accurate estimates. In the simulation study, we demonstrated that the bias correction leads to better estimates. Finally, we introduced a bootstrap method to estimate standard errors in RICS, where images are resampled from the original stack of images to create new datasets. The motivation behind the introduction of the bootstrapped standard error comes from the observation that in some cases the traditional way of estimating standard errors for RICS by means of the residuals gives unrealistically small values. The explanation for such small estimates could be that the residuals are highly correlated.

4.2 Paper II: Raster image analysis of diffusion for particle mixtures

In this study we extended the work done in Paper I to mixtures of particles. In SPRIA, the motion of each single particle is estimated, and we gain information about the distribution of the mean square displacement and functions that depend on it. As the mathematical model used for pure diffusion corresponds to a particle performing a Brownian motion, the theoretical distribution of the estimated diffusion coefficients can be computed, and involves a gamma distribution with parameters depending on the true diffusion coefficient and the length of the trajectory observed. We set up a maximum likelihood method to detect mixture models and estimate the diffusion coefficients of the different populations. In the validation study SPRIA has shown to give good estimates, but some caution must be taken when selecting the number of components in the mixture. When using criteria based on likelihood improvement, the maximum suggested number of components in the mixture is always selected, indicating that the likelihood is too sensitive to variability in the distribution of the diffusion coefficient. Thus, a complementary condition was necessary, where we rejected components for which the estimated proportion fell below a threshold. We also found that when applying RICS to such complex systems of mixtures of particles, a rather large difference between the components in the mixture was needed to allow identifiability. Thus, we investigated the use of RICS for mixtures by looking in more detail at the correlation function for different models involving diffusion to quantify how large the difference between the diffusion coefficients of each component need to be.

5 Future work

A natural extension of the present work is to apply SPRIA and compare it with ICS methods on heterogeneous samples with spatially varying mass transport properties. To this end, we have started to look at boundary effects to better understand the dynamics of molecules close to the transition phase in phase separated systems. More specifically, the interphase region in polymer networks and gels between the two phases typically presents a network like structure consisting of strands from the gel phase and voids. The network of strands becomes less dense the further away we move from the gel. Thus, mass transport properties like diffusion will be altered by the interphase region, changing from the behaviour expected in the gel phase to the one expected in the other phase. In a simple heterogeneous simulation example presented in Paper I, we have already shown that SPRIA could be applicable to complex systems. There, we imagined a sample made of two media, one characterized by low mobility and the other by high mobility of particles, and that the particles could move freely between the two. In particular, the case of a circular boundary between the two media has been considered. Such a situation could provide a simple model for e.g. an oil drop in water.

Concerning Paper II, at present we do not allow interactions between molecules of different subpopulations. The theory for SPRIA would be rather easy to extend to cover a diffusion-reaction process by means of the dependence of the mean square displacement on time. Similarly, a microrheology study could be performed to explore rheological properties of the medium such as viscoelasticity.

Another interesting topic would be to further investigate model selection criteria for both SPRIA and RICS. For SPRIA, the likelihood provides a direct way to measure performance of different models, but as presented in Paper II, it often overfits the data. In the case of RICS instead, residuals can be used to determine the most appropriate model by using cross-validation. Overall, resampling techniques like bootstrap could play a major role, as in SPRIA we have independent particles and in RICS independent images which could be used to produce new samples.

Appendices

A Derivation of RICS correlation function for pure diffusion

In this appendix we derive the formula for the correlation function given in Equation (3.1). In all correlation spectroscopy techniques, the signals fluctuation with respect to the average is calculated as

$$\delta F(r, t) = F(r, t) - \langle F(r, t) \rangle,$$

where $F(r, t)$ is the signal in r at time t , $\delta F(r, t)$ is the fluctuation of the signal and $\langle \cdot \rangle$ denotes averaging. The normalised correlation of the fluctuations, $G(\rho, \tau)$, is given by:

$$G(\rho, \tau) = \frac{\langle \delta F(r, t) \delta F(r + \rho, t + \tau) \rangle}{\langle F(r, t) \rangle^2} = \frac{\langle F(r, t) F(r + \rho, t + \tau) \rangle}{\langle F(r, t) \rangle^2} - 1,$$

where ρ and τ are the spatial and temporal shifts. First we derive the expression for the non-normalised correlation, $g(\rho, \tau)$,

$$g(\rho, \tau) = \langle \delta F(r, t) \delta F(r + \rho, t + \tau) \rangle. \quad (\text{A.1})$$

Fluctuations in the fluorescence signal are related to fluctuations in the concentration of particles, $\delta C(r, t)$, by

$$\delta F(r, t) = \int W(u) \eta \delta C(r - u, t) du, \quad (\text{A.2})$$

where η is a parameter that accounts for the collection efficiency of the setup, considered to be constant. $W(r)$ is the point-spread function. Using equations (A.1) and (A.2)

$$\begin{aligned} g(\rho, \tau) &= \left\langle \int W(u) \eta \delta C(r - u, t) du \int W(u') \eta \delta C(r + \rho - u', t + \tau) du' \right\rangle \\ &= \eta^2 \int \int \langle W(u) \delta C(r - u, t) W(u') \delta C(r + \rho - u', t + \tau) \rangle du du' \\ &= \eta^2 \int W(u) \int W(u') \langle \delta C(r - u, t) \delta C(r + \rho - u', t + \tau) \rangle du' du \end{aligned} \quad (\text{A.3})$$

Let $P(\rho, \tau)$ be the propagator for the given type of movement. Suppose we can show that

$$\langle \delta C(r, t) \delta C(r + \rho, t + \tau) \rangle = \langle C \rangle P(\rho, \tau) \quad (\text{A.4})$$

Then using equation (A.4), the equation (A.3) becomes

$$\begin{aligned} g(\rho, \tau) &= \langle C \rangle \eta^2 \int W(u) \int W(u') P(u - u' + \rho, \tau) du' du \\ &= \langle C \rangle \eta^2 \int W(u) (W(u + \rho) \otimes P(u + \rho, \tau)) du \end{aligned} \quad (\text{A.5})$$

where $W(u + \rho) \otimes P(u + \rho, \tau) = \int W(u') P(u - u' + \rho, \tau) du'$ is a convolution.

Now since the PSF is an even function, $W(u) = W(-u)$ and

$$\begin{aligned} g(\rho, \tau) &= \langle C \rangle \eta^2 \int W(u) (W(u + \rho) \otimes P(u + \rho, \tau)) du \\ &= \langle C \rangle \eta^2 \int W(-u) (W(u + \rho) \otimes P(u + \rho, \tau)) du \\ &= \langle C \rangle \eta^2 [W(\rho) \otimes (W(\rho) \otimes P(\rho, \tau))] \\ &= \langle C \rangle \eta^2 [(W(\rho) \otimes W(\rho)) \otimes P(\rho, \tau)], \end{aligned} \quad (\text{A.6})$$

where in the last line we applied the associativity of convolution. Now the average signal is given by

$$\langle F(r, t) \rangle = \left\langle \int W(u) \eta C(r - u, t) du \right\rangle = \eta \langle C \rangle.$$

The normalised correlation is given by

$$G(\rho, \tau) = \frac{(W(\rho) \otimes W(\rho)) \otimes P(\rho, \tau)}{\langle C \rangle}. \quad (\text{A.7})$$

We will now prove (A.4) for diffusing particles. Let us consider a solution with m different components with diffusion coefficients D_j , $j = 1, \dots, m$. Let $C_j(r, t)$ denote the concentration in r at time t of the j -th component. Furthermore, let $\bar{C}_j = \langle C_j(r, t) \rangle$ and again $\delta C_j(r, t) = C_j(r, t) - \bar{C}_j$. Due to the fact that we are considering diffusion, both the concentration of particles and the fluctuations will satisfy the diffusion equation

$$\frac{\partial u(r, t)}{\partial t} = D \nabla^2 u(r, t)$$

which in our case means

$$\frac{\partial \delta C_j(r, t)}{\partial t} = D_j \nabla^2 \delta C_j(r, t). \quad (\text{A.8})$$

Now the zero-time correlations $\langle \delta C_j(r, 0) \delta C_k(r'', 0) \rangle$ can be evaluated by taking advantage of the following properties of the solution: the correlation length is much smaller than the distances between molecules, the positions of different molecules of the same species as well as those of different species are uncorrelated:

$$\langle \delta C_j(r, 0) \delta C_k(r'', 0) \rangle = \bar{C}_j \delta_{jk} \delta(r - r'') \quad (\text{A.9})$$

In order to obtain the solution $\delta C_j(r, t)$ as a function of the initial conditions $\delta C_j(r, 0)$ we apply a Fourier transform to equation (A.8):

$$\frac{d\tilde{C}_l(q, t)}{dt} = \sum_{k=1}^m M_{lk} \tilde{C}_k(q, t) \quad (\text{A.10})$$

where $\tilde{C}_l(q, t) = (2\pi)^{-\frac{3}{2}} \int \delta C_l(r, t) e^{iqr} dr$ is the Fourier transform of $\delta C_l(r, t)$, and $M_{lk} = \delta_{lk} D_l q^2$. That is, $M = [M_{lk}]$ is a diagonal matrix with eigenvalues $\lambda_l = -D_l q^2$ for $l = 1, \dots, m$ and the corresponding eigenvectors are

$$e_l = [0, \dots, 0, \underbrace{1}_{l\text{-th element}}, 0, \dots, 0]$$

The solutions of (A.10) can be represented through eigenvalues and eigenvectors of M by:

$$\tilde{C}_l(q, t) = h_l e^{-D_l q^2 t} \quad (\text{A.11})$$

The coefficients h_l are to be found from the initial conditions: $\tilde{C}_l(q, 0) = h_l$ and so

$$\tilde{C}_l(q, t) = \tilde{C}_l(q, 0) e^{-D_l q^2 t} \quad (\text{A.12})$$

With the same reasoning we can obtain

$$\tilde{C}_l(q, t + \tau) = \tilde{C}_l(q, t) e^{-D_l q^2 \tau} \quad (\text{A.13})$$

and

$$\delta C_l(r, t) = (2\pi)^{-\frac{3}{2}} \int \tilde{C}_l(q, t) e^{-iqr} dq. \quad (\text{A.14})$$

Now taking into account that Fourier transform and averaging can be applied

in any order, we get

$$\begin{aligned}
\langle \delta C_j(r, t) \delta C_l(r + \rho, t + \tau) \rangle &= (2\pi)^{-\frac{3}{2}} \int \langle \delta C_j(r, t) \tilde{C}_l(q, t + \tau) \rangle e^{-iq(r+\rho)} dq = \\
&= (2\pi)^{-\frac{3}{2}} \int \langle \delta C_j(r, t) \tilde{C}_l(q, t) \rangle e^{-D_l \tau q^2} e^{-iq(r+\rho)} dq = \\
&= (2\pi)^{-3} \int e^{-D_l \tau q^2} e^{-iq(r+\rho)} \int \langle \delta C_j(r, t) \delta C_l(r'', t) \rangle e^{iqr''} dr'' dq = \\
&= (2\pi)^{-3} \bar{C}_l \delta_{jl} \int e^{-D_l \tau q^2} e^{-iq(r+\rho)} e^{iqr} dq = \\
&= (2\pi)^{-3} \bar{C}_l \delta_{jl} \int e^{-D_l \tau q^2} e^{-iq\rho} dq = \\
&= (2\pi)^{-3} \bar{C}_l \delta_{jl} \int e^{-D_l \tau q_1^2} e^{-iq_1 \rho_1} dq_1 \int e^{-D_l \tau q_2^2} e^{-iq_2 \rho_2} dq_2 \int e^{-D_l \tau q_3^2} e^{-iq_3 \rho_3} dq_3 = \\
&= (2\pi)^{-3} \bar{C}_l \delta_{jl} \left(\sqrt{\frac{\pi}{D_l \tau}} \right)^3 e^{-\frac{\rho_1^2 + \rho_2^2 + \rho_3^2}{4D_l \tau}} = \\
&= \bar{C}_l \delta_{jl} \left(\frac{1}{\sqrt{4\pi D_l \tau}} \right)^3 e^{-\frac{\rho^2}{4D_l \tau}} = \\
&= \bar{C}_l \delta_{jl} P(\rho, \tau)
\end{aligned} \tag{A.15}$$

where on line 1 we exchanged the order of Fourier and average and used (A.14) with $r+\rho$ and $t+\tau$ in place of r and t . On line 2 we used equation (A.13). On line 3 we utilized $\langle \delta C_j(r, t) \delta C_l(r'', t) \rangle = \bar{C}_l \delta_{jl} \delta r - r''$ by (A.9) and on line 4 we used that $\int e^{iqr''} \delta(r - r'') dr'' = e^{iqr}$. On line 6 we splitted the integral into a product of single component integrals. On line 7 we used that $\int e^{-D_l \tau q_1^2} e^{-iq_1 \rho_1} dq_1 = \sqrt{\frac{\pi}{D_l \tau}} e^{-\frac{\rho_1^2}{4D_l \tau}}$ by Fourier transform of a Gaussian distribution, and the same for the other two integrals.

We can now use the computation above to compute the correlation function for RICS in case of diffusion. Recall that the normalised correlation is given by

$$G(\rho, \tau) = \frac{(W(\rho) \otimes W(\rho)) \otimes P(\rho, \tau)}{\langle C \rangle},$$

where the PSF is

$$W(r) = \frac{\left(\frac{2}{\pi}\right)^{3/2}}{w_0^2 w_z} \exp\left(-2\frac{r_x^2 + r_y^2}{w_0^2} - 2\frac{r_z^2}{w_z^2}\right)$$

and the propagator is

$$P(\rho, \tau) = \frac{1}{(\sqrt{4\pi D\tau})^3} \exp\left(-\frac{\rho_x^2 + \rho_y^2 + \rho_z^2}{4D\tau}\right).$$

Now if we write down the normalised correlation with the above expression for P and W we get (the constant has changed using $\langle C \rangle \pi^{\frac{3}{2}} w_0^2 w_z = \langle N \rangle$)

$$\begin{aligned} G(\rho, \tau) &= \frac{1}{\langle N \rangle (\sqrt{4\pi D\tau})^3} \iiint \exp\left[-\frac{a^2 + b^2}{w_0^2} - \frac{c^2}{w_z^2}\right] \times \\ &\quad \times \exp\left[-\frac{(\rho_x - a)^2 + (\rho_y - b)^2 + (\rho_z - c)^2}{4D\tau}\right] da db dc = \\ &= \frac{1}{M} \iiint e^{-\frac{(w_0^2 + 4D\tau)a^2 - 2w_0^2\rho_x a + w_0^2\rho_x^2}{w_0^2 4D\tau} - \frac{(w_0^2 + 4D\tau)b^2 - 2w_0^2\rho_y b + w_0^2\rho_y^2}{w_0^2 4D\tau}} \times \\ &\quad \times e^{-\frac{(w_z^2 + 4D\tau)c^2 - 2w_z^2\rho_z c + w_z^2\rho_z^2}{w_z^2 4D\tau}} da db dc \end{aligned} \quad (\text{A.16})$$

where $M = \langle N \rangle (\sqrt{4\pi D\tau})^3$. Then by separating the integral with respect to each variable we obtain

$$\begin{aligned} G(\rho, \tau) &= \frac{1}{M} \int e^{-\frac{(w_0^2 + 4D\tau)a^2 - 2w_0^2\rho_x a + w_0^2\rho_x^2}{w_0^2 4D\tau}} da \int e^{-\frac{(w_0^2 + 4D\tau)b^2 - 2w_0^2\rho_y b + w_0^2\rho_y^2}{w_0^2 4D\tau}} db \times \\ &\quad \times \int e^{-\frac{(w_z^2 + 4D\tau)c^2 - 2w_z^2\rho_z c + w_z^2\rho_z^2}{w_z^2 4D\tau}} dc. \end{aligned} \quad (\text{A.17})$$

Now just focus on the first integral term in the above product and rewrite the exponent to get:

$$\int e^{-\frac{(w_0^2 + 4D\tau)a^2 - 2w_0^2\rho_x a + w_0^2\rho_x^2}{w_0^2 4D\tau}} da = \int e^{-\frac{a^2 - \frac{2w_0^2\rho_x}{w_0^2 + 4D\tau}a + \frac{w_0^2\rho_x^2}{w_0^2 + 4D\tau}}{\frac{w_0^2 4D\tau}{w_0^2 + 4D\tau}}} da := (**)$$

Observe now that the numerator in the exponential can be written as

$$a^2 - \frac{2w_0^2\rho_x}{w_0^2 + 4D\tau}a + \frac{w_0^2\rho_x^2}{w_0^2 + 4D\tau} = a^2 - \frac{2w_0^2\rho_x}{w_0^2 + 4D\tau}a + \frac{w_0^2\rho_x^2}{w_0^2 + 4D\tau} \pm \frac{w_0^4\rho_x^2}{(w_0^2 + 4D\tau)^2} =$$

$$= \left(a - \frac{w_0^2 \rho_x}{w_0^2 + 4D\tau} \right)^2 + \frac{w_0^2 \rho_x^2}{w_0^2 + 4D\tau} - \frac{w_0^4 \rho_x^2}{(w_0^2 + 4D\tau)^2}$$

then

$$\begin{aligned} (**) &= \int \exp \left[-\frac{\left(a - \frac{w_0^2 \rho_x}{w_0^2 + 4D\tau} \right)^2}{\frac{w_0^2 + 4D\tau}{w_0^2 + 4D\tau}} - \frac{\frac{w_0^2 \rho_x^2}{w_0^2 + 4D\tau} - \frac{w_0^4 \rho_x^2}{(w_0^2 + 4D\tau)^2}}{\frac{w_0^2 + 4D\tau}{w_0^2 + 4D\tau}} \right] da = \\ &= \exp \left[-\frac{w_0^4 \rho_x^2 + 4D\tau w_0^2 \rho_x^2 - w_0^4 \rho_x^2}{(w_0^2 + 4D\tau)(w_0^2 + 4D\tau)} \right] \int \exp \left[-\frac{\left(a - \frac{w_0^2 \rho_x}{w_0^2 + 4D\tau} \right)^2}{\frac{w_0^2 + 4D\tau}{w_0^2 + 4D\tau}} \right] da = \end{aligned}$$

(multiply and divide by $\sqrt{\pi \frac{w_0^2 + 4D\tau}{w_0^2 + 4D\tau}}$)

$$\begin{aligned} &= e^{-\frac{\rho_x^2}{w_0^2 + 4D\tau}} \int \frac{\sqrt{\pi \frac{w_0^2 + 4D\tau}{w_0^2 + 4D\tau}}}{\sqrt{\pi \frac{w_0^2 + 4D\tau}{w_0^2 + 4D\tau}}} \exp \left[-\frac{\left(a - \frac{w_0^2 \rho_x}{w_0^2 + 4D\tau} \right)^2}{\frac{w_0^2 + 4D\tau}{w_0^2 + 4D\tau}} \right] da = \\ &= e^{-\frac{\rho_x^2}{w_0^2 + 4D\tau}} \sqrt{\pi \frac{w_0^2 + 4D\tau}{w_0^2 + 4D\tau}} \int \frac{1}{\sqrt{\pi \frac{w_0^2 + 4D\tau}{w_0^2 + 4D\tau}}} \exp \left[-\frac{\left(a - \frac{w_0^2 \rho_x}{w_0^2 + 4D\tau} \right)^2}{\frac{w_0^2 + 4D\tau}{w_0^2 + 4D\tau}} \right] da. \end{aligned}$$

But

$$f(a) = \frac{1}{\sqrt{\pi \frac{w_0^2 + 4D\tau}{w_0^2 + 4D\tau}}} \exp \left[-\frac{\left(a - \frac{w_0^2 \rho_x}{w_0^2 + 4D\tau} \right)^2}{\frac{w_0^2 + 4D\tau}{w_0^2 + 4D\tau}} \right]$$

is the density of a normal distribution, $\mathcal{N}\left(\frac{w_0^2 \rho_x}{w_0^2 + 4D\tau}, \frac{w_0^2 + 4D\tau}{w_0^2 + 4D\tau}\right)$, and hence

$$\int f(a) da = 1.$$

This implies that

$$\int e^{-\frac{(w_0^2 + 4D\tau)a^2 - 2w_0^2 \rho_x a + w_0^2 \rho_x^2}{w_0^2 + 4D\tau}} da = e^{-\frac{\rho_x^2}{w_0^2 + 4D\tau}} \sqrt{\pi \frac{w_0^2 + 4D\tau}{w_0^2 + 4D\tau}}.$$

With a similar computation we can get the second and third integrals in the expression of the normalised correlation:

$$\int e^{-\frac{(w_0^2+4D\tau)b^2-2w_0^2\rho_y b+w_0^2\rho_y^2}{w_0^2 4D\tau}} db = e^{-\frac{\rho_y^2}{w_0^2+4D\tau}} \sqrt{\pi \frac{w_0^2 4D\tau}{w_0^2+4D\tau}}$$

and

$$\int e^{-\frac{(w_z^2+4D\tau)c^2-2w_z^2\rho_z c+w_z^2\rho_z^2}{w_z^2 4D\tau}} dc = e^{-\frac{\rho_z^2}{w_z^2+4D\tau}} \sqrt{\pi \frac{w_z^2 4D\tau}{w_z^2+4D\tau}}$$

We can now rewrite the correlation function

$$\begin{aligned} G(\rho, \tau) &= \frac{1}{M} \int e^{-\frac{(w_0^2+4D\tau)a^2-2w_0^2\rho_x a+w_0^2\rho_x^2}{w_0^2 4D\tau}} da \int e^{-\frac{(w_0^2+4D\tau)b^2-2w_0^2\rho_y b+w_0^2\rho_y^2}{w_0^2 4D\tau}} db \times \\ &\quad \times \int e^{-\frac{(w_z^2+4D\tau)c^2-2w_z^2\rho_z c+w_z^2\rho_z^2}{w_z^2 4D\tau}} dc = \\ &= \frac{1}{M} e^{-\frac{\rho_x^2}{w_0^2+4D\tau}} e^{-\frac{\rho_y^2}{w_0^2+4D\tau}} \left(\pi \frac{w_0^2 4D\tau}{w_0^2+4D\tau} \right) e^{-\frac{\rho_z^2}{w_z^2+4D\tau}} \sqrt{\pi \frac{w_z^2 4D\tau}{w_z^2+4D\tau}} \end{aligned} \quad (\text{A.18})$$

Now we can use the fact that imaging is done in a two-dimensional plane, so we will consider only the case $\rho = (\rho_x, \rho_y, 0)$ and so

$$\begin{aligned} G(\rho, \tau) &= \frac{1}{\langle N \rangle (\sqrt{4\pi D\tau})^3} e^{-\frac{\rho_x^2}{w_0^2+4D\tau}} e^{-\frac{\rho_y^2}{w_0^2+4D\tau}} \left(\pi \frac{w_0^2 4D\tau}{w_0^2+4D\tau} \right) \sqrt{\pi \frac{w_z^2 4D\tau}{w_z^2+4D\tau}} = \\ &= \frac{1}{\langle N \rangle} e^{-\frac{\rho_x^2+\rho_y^2}{w_0^2+4D\tau}} \left(\pi \frac{w_0^2 4D\tau}{w_0^2+4D\tau} \frac{1}{4D\tau} \right) \sqrt{\pi \frac{w_z^2 4D\tau}{w_z^2+4D\tau} \frac{1}{\pi 4D\tau}} = \\ &= \frac{1}{\langle N \rangle} e^{-\frac{\rho_x^2+\rho_y^2}{w_0^2+4D\tau}} \left(\pi \frac{w_0^2 4D\tau}{w_0^2+4D\tau} \frac{1}{\pi 4D\tau} \right) \sqrt{\pi \frac{w_z^2 4D\tau}{w_z^2+4D\tau} \frac{1}{\pi 4D\tau}} = \\ &= \frac{1}{\langle N \rangle} e^{-\frac{\rho_x^2+\rho_y^2}{w_0^2+4D\tau}} \left(\frac{w_0^2}{w_0^2+4D\tau} \right) \sqrt{\frac{w_z^2}{w_z^2+4D\tau}} = \\ &= \frac{1}{\langle N \rangle} e^{-\frac{\rho_x^2+\rho_y^2}{w_0^2+4D\tau}} \left(\frac{w_0^2+4D\tau}{w_0^2} \right)^{-1} \left(\frac{w_z^2+4D\tau}{w_z^2} \right)^{-\frac{1}{2}} = \\ &= \frac{1}{\langle N \rangle} e^{-\frac{\rho_x^2+\rho_y^2}{w_0^2+4D\tau}} \left(1 + \frac{4D\tau}{w_0^2} \right)^{-1} \left(1 + \frac{4D\tau}{w_z^2} \right)^{-\frac{1}{2}} \end{aligned} \quad (\text{A.19})$$

To get the final form it is enough to substitute above $\tau = \tau_p|\xi| + \tau_l|\psi|$ and $\rho_x = S\xi$, $\rho_y = S\psi$, where S is the pixel size and ξ and ψ are, respectively, the x and y axis spatial increments in the number of pixels:

$$G(\xi, \psi) = \frac{1}{\langle N \rangle} e^{\left[-\frac{(S\xi)^2 + (S\psi)^2}{w_0^2 + 4D(\tau_p|\xi| + \tau_l|\psi|)} \right]} \left(1 + \frac{4D(\tau_p|\xi| + \tau_l|\psi|)}{w_0^2} \right)^{-1} \times \quad (\text{A.20})$$

$$\times \left(1 + \frac{4D(\tau_p|\xi| + \tau_l|\psi|)}{w_z^2} \right)^{-\frac{1}{2}}.$$

Thus, we have obtained equation 3.1.

References

- Bouchard, J. & Georges, A. (1990) Anomalous diffusion in disordered media: statistical mechanisms, models and physical applications. *Physics Reports*, **195**, 127–293.
- Brown, C. M., Dalal, R. B., Herbert, B., Digman, M. A., Horwitz, A. R. & Gratton, E. (2008) Raster image correlation spectroscopy (RICS) for measuring fast protein dynamics and concentrations with a commercial laser scanning confocal microscope. *Journal of Microscopy*, **229**, 78–91.
- Comeau, J. W., Costantino, S. & Wiseman, P. W. (2006) A guide to accurate fluorescence microscopy colocalization measurements. *Biophysical Journal*, **89**, 1251–1260.
- Digman, M. A., Brown, C. M., Sengupta, P., Wiseman, P. W., Horwitz, A. R. & Gratton, E. (2005) Measuring fast dynamics in solutions and cells with a laser scanning microscope. *Biophysical Journal*, **89**, 1317–1327.
- Einstein, A. (1905) Über die von Molekularkinetischen Theorie der Wärme geforderte Bewegung von in ruhenden Flüssigkeiten suspendierten Teilchen. *Annalen der Physik*, **8**, 549–560.
- Gielen, E., Smisdom, N., Vandeven, M., De Clercq, B., Gratton, E., Digman, M., Rigo, J.-M., Hofkens, J., Engelborghs, Y. & Ameloot, M. (2009) Measuring diffusion of lipid-like probes in artificial and natural membranes by raster image correlation spectroscopy (RICS): use of a commercial laser-scanning microscope with analog detection. *Langmuir*, **25**, 5209–5218.
- Hebert, B., Costantino, S. & Wiseman, P. W. (2005) Spatiotemporal image correlation spectroscopy (STICS) theory, verification, and application to protein velocity mapping in living CHO cells. *Biophysical Journal*, **88**, 3601–3614.
- Kolin, D. L., Ronis, D. & Wiseman, P. W. (2006) K-space image correlation spectroscopy: a method for accurate transport measurements independent of fluorophore photophysics. *Biophysical Journal*, **91**, 3061–3075.
- Kulkarni, R., Wu, D., Davis, M. E. & Fraser, S. E. (2005) Quantitating intracellular transport of polyplexes by spatio-temporal image correlation spectroscopy. *Proc. Natl. Acad. Sci. U.S.A.*, **102**, 7523–7528.

- Lorén, N., Hagman, J., Jonasson, J. K., Deschout, H., Bernin, D., Cellaz-Zanacchi, F., Diaspro, A., McNally, J. G., Ameloot, M., Smisdom, N., Nydén, M., Hermansson, A.-M., Rudemo, M. & Braeckmans, K. (2015) Fluorescence recovery after photobleaching in material and life sciences: putting theory into practice. *Quarterly Reviews of Biophysics*, **48**, 323–387.
- Pawley, J. B. (2006) *Handbook of Biological Confocal Microscopy*. Springer Science, New York.
- Perrin, J. (1909) Mouvement brownien et réalité moléculaire. *Ann. Chem. Phys.*, **18**, 5–114.
- Schuster, E., Sott, K., , Ström, A., Altskär, A., Smisdom, N., Lorén, N. & Hermansson, A.-M. (2016) Interplay between flow and diffusion in capillary alginate hydrogels. *Soft Matter*, **12**, 3897–3907.
- Smoluchowski, M. (1906) Zur kinetischen Theorie der Brownschen Molekularbewegung und der Suspensionen. *Annalen der Physik*, **14**, 756–780.